Supporting Information (SI)

Design optimization of energized composite for electric vehicles using simulation and experimental methods

Deepak Pandey[1,2], Rajkumar Gurjar[1,2], Kowsik Sambath Kumar[1,2], Leaford Nathan Henderson[1,2], Maydenee Maydur Tresa[1,2], Luke Roberson[3], A. Mohammed Hussain [4], Nilesh Dale[4] and Jayan Thomas*[1,2,5]

[1]Department of Materials Science and Engineering, University of Central Florida, Orlando, Florida 32816, United States
[2]NanoScience Technology Center, University of Central Florida, Orlando, Florida 32826, United States
[3]NASA Kennedy Space Center, FL, 32899, USA
[4]Nissan Technical CenterNorth America, 39001 Sunrise Drive, Farmington Hills, Michigan 48331, United States
[5]CREOL, College of Optics and Photonics, University of Central Florida, Orlando, Florida 32816, United States.

[*]E-mail: Jayan.Thomas@ucf.edu

1. FEA Model selection and theory

1.1 FEA model selection

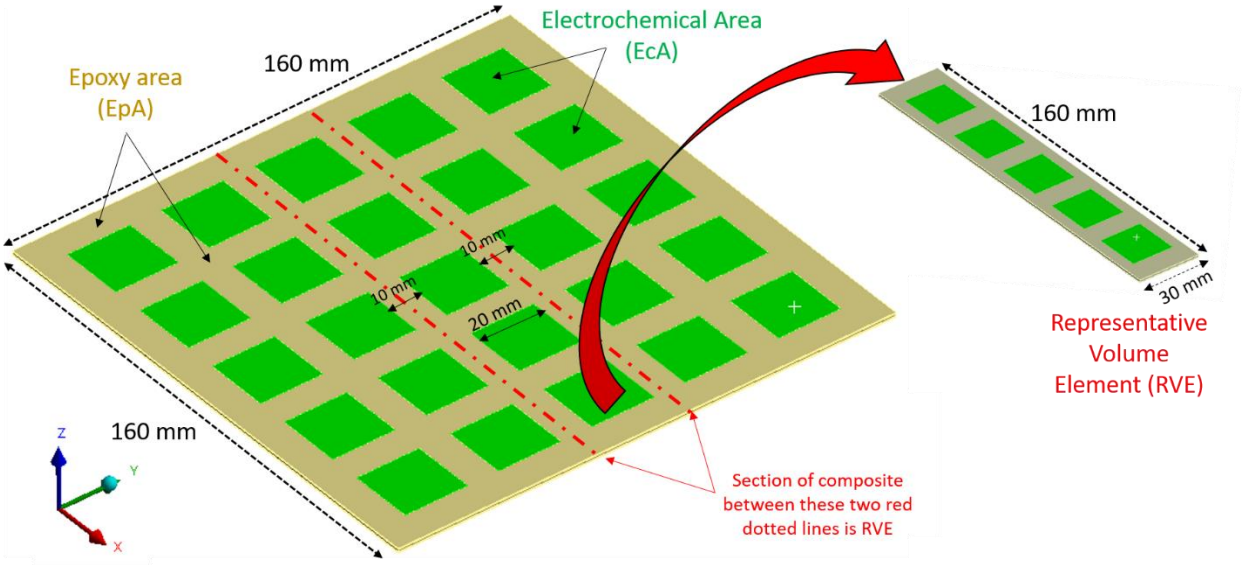

Figure S1. A representative volume element (REV) of 160 mm × 30 mm area from a 160 mm ×160 mm energized composite lamina. 7 such laminas after layup process would make a 2.3 mm thick composite REV. This REV can be easily fabricated and tested on a UTM since it is in a bar shape and has dimensions closer to ASTM D3039 (Tensile test) and ASTM D 790 (flexural test).

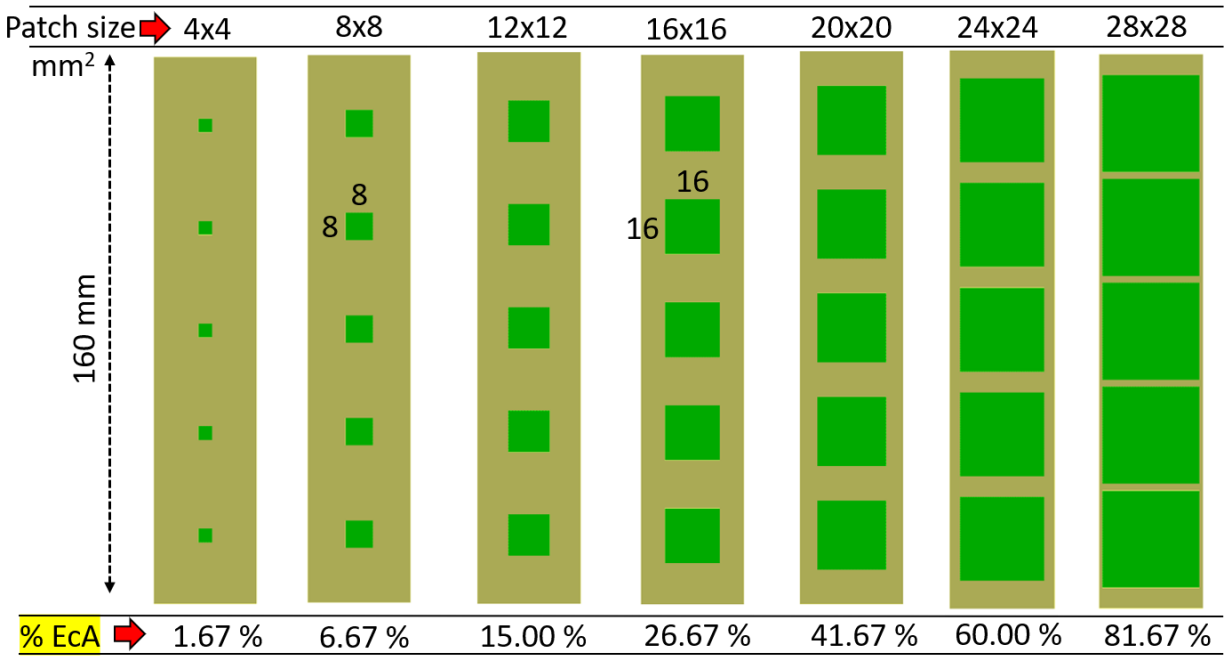

Figure S2. 7 Different configurations of energized composite (in the form of REVs) having electrode patch area ranging from 28×28, 24×24, 20×20, 16×16, 12×12, 8×8, and 4×4 mm^2. All of these configurations have been fabricated in the form of a composite bar of 2.3 mm thickness. They have been simulated in same size for their bending and tensile strengths and experimentally tested as well for confirmation.

1.2 Maximum stress damage model:

The maximum stress criterion, the ratio of actual stresses to failure stresses are compared in the ply principal coordinate system. This criterion is based on the stress in one component, hence can also be considered as a non-interactive stress damage criterion.[1] The maximum stress criterion can be described with the following equation:

$$f = \max\left(\left|\frac{\sigma_1}{X}\right|, \left|\frac{\sigma_2}{Y}\right|, \left|\frac{\sigma_3}{Z}\right|, \left|\frac{\tau_{12}}{S_{12}}\right|, \left|\frac{\tau_{13}}{S_{13}}\right|, \left|\frac{\tau_{23}}{S_{23}}\right|\right);\ f \geq 1 \text{ indicate the damage}$$

$$\sigma_1 \geq 0 \Longrightarrow X = X_t \ ; \qquad \sigma_1 < 0 \Longrightarrow X = X_c$$
$$\sigma_2 \geq 0 \Longrightarrow Y = Y_t \ ; \qquad \sigma_2 < 0 \Longrightarrow Y = Y_c$$
$$\sigma_3 \geq 0 \Longrightarrow Z = Z_t \ ; \qquad \sigma_3 < 0 \Longrightarrow Z = Z_c$$

where X_t, X_c, Y_t, Y_c, Z_t, Z_c S_{12}, S_{13} and S_{23} represent the axial tensile strength, axial compressive strength, transverse tensile strength, transverse compressive strength, out of plane tensile strength, out of plane compressive strength, transverse shear strength and two axial shear strengths, respectively. Damage index ($f \geq 1$) leads to the degradation of the laminates in the form of materials stiffness. The evolution of damage is characterized by the material property degradation in engineering data.[2] The material property degradation coefficients are given in Table S1.

Table S1: Damage evolution model parameters for energized composites[2, 3]

Parameter	Value
Tensile fiber stiffness reduction	.07
Compressive fiber stiffness reduction	.14
Tensile matrix stiffness reduction	1
Compressive matrix stiffness reduction	1

1.3 Cohesive Zone Model (CZM):

The ideal bilinear traction-separation softening cohesive zone model (CZM) enables a prediction of the stress-strain behavior of the adhesive interface.[4] The bilinear cohesive law with the mixed-mode failure is applied to the interface adhesive surface of laminates. For bilinear cohesive law under the mixed-mode fracture, the separation of material interfaces depends on both the normal and tangential components of displacement jumps.[5] The interface is loaded elastically till the maximum traction point and then followed by linear softening. The theory for CZM mixed mode delamination is explained by [6]

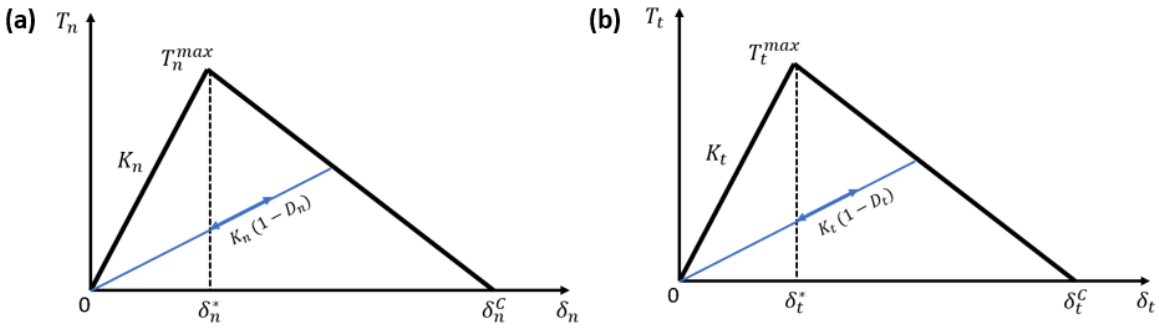

Figure S3: Traction separation laws for cohesive interface elements for (a) Mode-I, (b) Mode-II

The normal and tangent components of the cohesive tractions are defined as

$$T_n = K_n \delta_n (1 - D_n)$$
$$T_t = K_t \delta_t (1 - D_t)$$

Where K_n and K_t are the normal and tangential cohesive stiffness values. D_n and D_t are the damage variables ranging between 0 and 1. The interface remains intact at the 0 value of D_m. δ_n^C and δ_t^C are normal and tangential displacement jumps respectively at the completion of

debonding. The damage of interface elements occurs once the elements satisfy the below equation:[7]

$$\left\{\frac{\tau_n}{N}\right\}^2 + \left\{\frac{\tau_s}{S}\right\}^2 + \left\{\frac{\tau_t}{S}\right\}^2 = 1$$

where τ_n is the normal stress and τ_s and τ_t are the shear stresses in other directions. N and S are the strength in normal and shear directions. Additionally, critical energy release rate based Benzeggah–Kenane criteria is integrated in damage evolution of the interface element as per the below equation.[8]

$$G_I^C + (G_I^C - G_{II}^C)\left\{\frac{G_{II} + G_{III}}{G_I + G_{II} + G_{III}}\right\}^{\alpha} = G^C$$

Therein, G^C represents the total critical energy release rate; α is the mode mixity parameter, while G_I, G_{II} and G_{III} are energy release rates for failure modes of mode I, II, and III respectively. The cohesive zone modeling properties of energized laminates are shown in Table S2.[9, 10]

Table S2: Interlaminar cohesive zone modelling parameters for energized composites [6, 9, 11]

Parameter	Maximum Normal Traction (T_n) [MPa]	Maximum Tangential Traction (T_t) [MPa]	Penalty stiffness (K_n & K_t) [N/mm^3]	Mode I fracture toughness (G_I^C) [J/m^2]	Mode II fracture toughness (G_{II}^C) [J/m^2]	Mode-mixity parameter
Value	50	75	10^6	350	740	1.45

2. Experimental Details

2.1 Fabrication of samples for flexural tests

Sample preparation: 6K, 2×2 Twill weave 5-yard carbon fiber roll was purchased from Fibreglast. This carbon fiber roll has been used to cut out carbon fiber sheets. Woven roving (#223-C) glass fiber roll from Fibreglast have been used as glass fiber sheets. All other materials have been kept same as that listed in our previous study.[12] As discussed in the simulation studies, 7 configurations with varying patch sizes: 28×28, 24×24, 20×20, 16×16, 12×12, 8×8, and 4×4 mm^2 were chosen for design optimization. Each of these composites will be fabricated with 4 carbon fibers (2 anodes and 2 cathodes) and 3 glass fiber (2 separator and 1 insulator) layers. In order to choose an appropriate dimension for design optimization studies, a 160 mm × 160 mm × 2.3 mm volume (based on 7 layers thickness) was chosen. However, since such a size cannot be experimentally tested on a UTM, thus a representative volume element (RVE) of 160 mm × 30 mm × 2.3 mm which was clearly a repeating unit was chosen which could be easily fabricated, simulated and experimentally tested on a UTM. Check Figure S1 and S2 in supporting information.

In order to fabricate the samples for flexural test, the same patterned approach was used as discussed in our previous study.[Ref][12] The electrode material was deposited in a square patch

shape on a 160 mm × 30 mm carbon fiber mat strips. Total 5 patch could be made on each of the carbon fiber strip. To fabricate a composite with reasonable thickness, 4 carbon fiber strips (2 anode and 2 cathode) and 3 glass fiber strips were alternated just like discussed in our previous study. This lead to a thickness of around 2.3 mm.

Total 7 such composites were made with a variation in their electrode area (square patch sizes): 28×28, 24×24, 20×20, 16×16, 12×12, 8×8, and 4×4 mm^2 (Check figure S3 below). While fabricating these composites it was ensured that the location of centers and number of patches remains unchanged in each of the configuration. Only the size of these patches was modulated which resulted in the desired variations of EcA vs EpA. Each of the layer in same composite were designed to have same configuration (patch sizes). The composite were fabricated using hand layup process and cured under compression molding just like in our previous study. Total 7 composites were made having the final dimensions of 160 mm × 30 mm × 2.3 mm

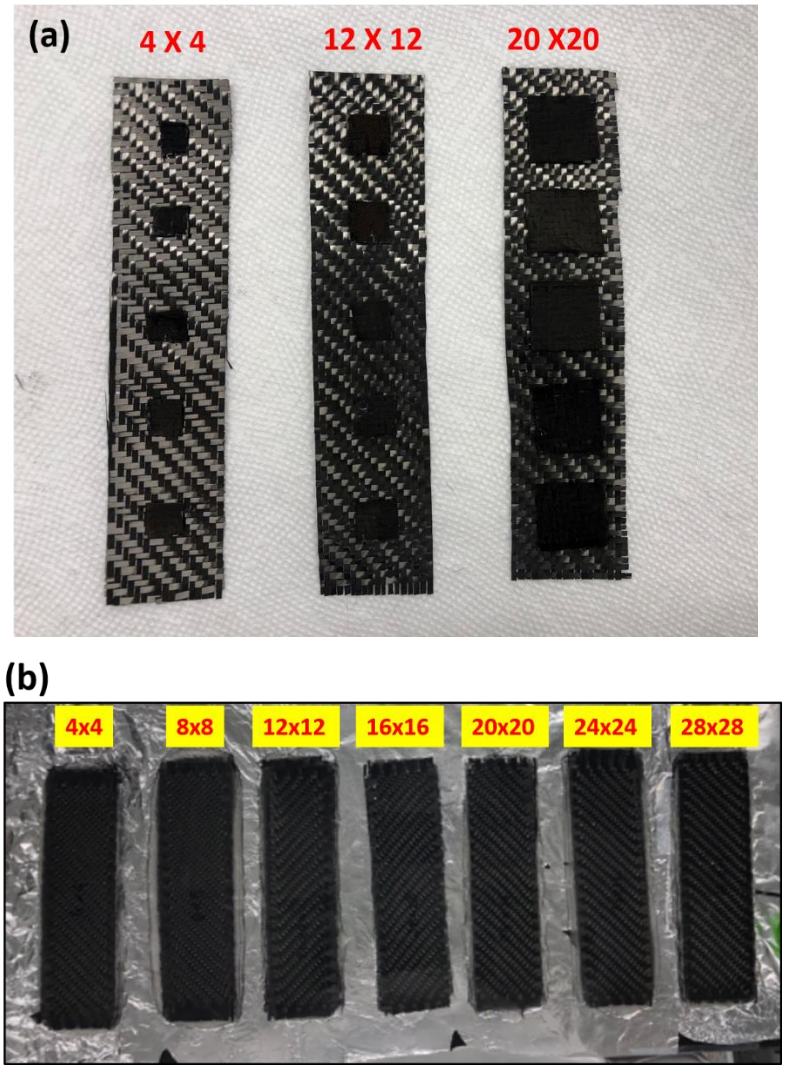

Figure S3. Experimental samples.(a) Image shows difference in patch sizes (EcA areas) for some of the various configurational energized composite single laminas before composite fabrication. (b) Fabricated

REVs of energized composite for different configurations, ready for test on UTM. 7 such composites are made of tensile tests and 7 for bending test.

2.2 Fabrication of samples for tensile tests

Sample preparation: Similar to the sample preparation of flexural tests, 7 configurations of energized composite with varying patch sizes (as discussed previously): 28×28, 24×24, 20×20, 16×16, 12×12, 8×8, and 4×4 mm^2 were fabricated for tension test. Each composite was fabricated using 4 carbon fibers (2 anodes and 2 cathodes) and 3 glass fiber (2 separator and 1 insulator) layers. Dimensions of these carbon and glass fiber strips were kept to match the representative volume element (RVE) of 160 mm × 30 mm as taken in the samples of bending tests. Total 7 layers would make up a thickness of ~ 2.3 mm. For fabricating the configured composites, same electrode patterning approach was used like we have discussed in the flexural test and also in our previous study.[12]

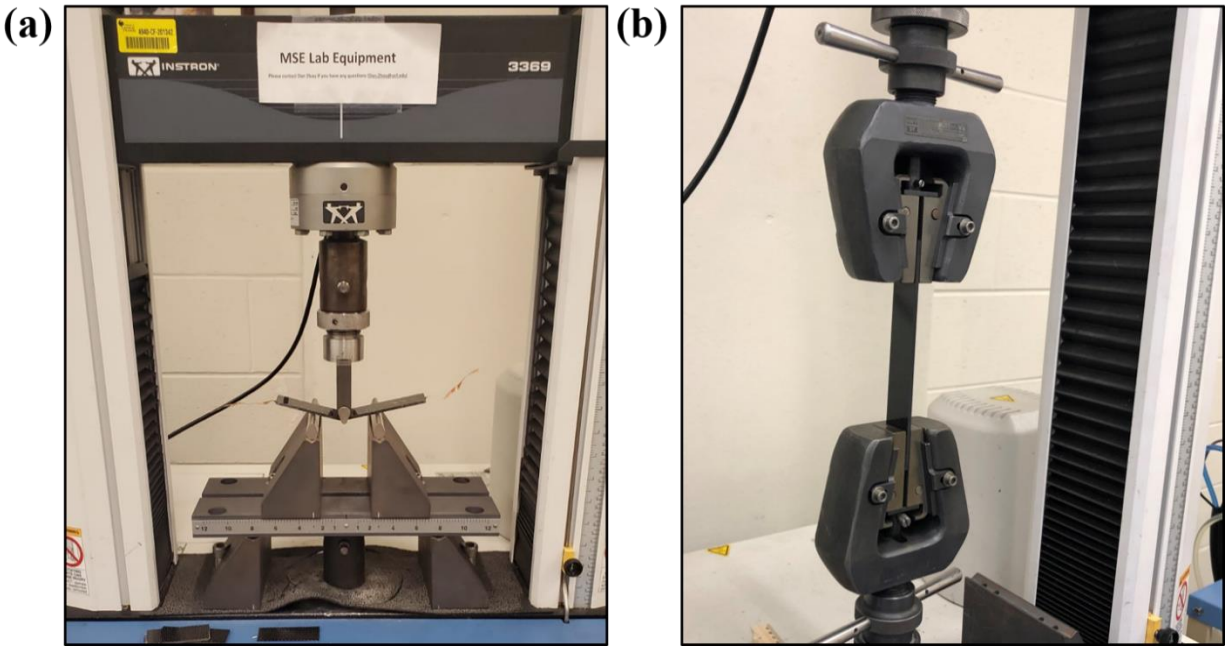

Figure S4. Experimental Tests (a) Image showing the energized composite sample being subjected to the 3-point bend test. (b) Image showing the energized composite sample subjected to uniaxial tension test.

Table S3. Similar reported energized composites compared with our design-optimized energized composite, for their respective mechanical and electrochemical performance.

Ref.	Other Energized Composites (electrode & electrolyte)	Electrochemical and Mechanical performance	Design optimized Energized Composite.[12]
[13]	• Carbon electrode coatings on the rigid honeycomb Al current collector walls. • 1M $TEABF_4$ in propylene carbonate (PC) electrolyte	• Max Energy density of 0.68 Wh m^{-2} and Power density of 30.5 W m^{-2} • Flammable organic electrolyte • Only designed for bending loads.	• Max Energy density of 2.5 Wh m^{-2} and Power density of 203 W m^{-2} • Non-flammable aqueous electrolyte • Takes both tension and bending loads
[14]	• Activated carbon (AC) casted on aluminum foils sandwiched with epoxy-carbon fiber mats. • PVDF, lithium triflate-epoxy binder	• Energy density of 2.64 Wh kg^{-1}, Cycle life (CL) 5000 • Tensile strength of only 80 MPa).	• Energy density of 33.12 Wh kg^{-1}. 8500 Cycles. • Max tensile strength of 552 MPa.
[15]	• Discontinuous carbon fiber (CF) dry prepegs electrodes • PVDF, lithium triflate and epoxy	• Areal capacitance of only 0.128 mF cm^{-2}. • Low flexural strength of 47.49 MPa, no tension test performed.	• Max areal capacitance of 550 mF cm^{-2}. • Max Flexural strength of 887.9 MPa. Tension test performed
[16]	• Nanoporous silicon interfaces electrodes. • Bisphenol A ionic liquid-epoxy resin as electrolyte	• Energy density of 5-8 Wh kg^{-1} and a low 4000 CL • Tensile strength of only 1 MPa	• Energy density of 33.12 Wh kg^{-1}. High 8500 CL • Max tensile strength of 552 MPa
[17]	• Activated carbon fiber mat as electrodes. • Ethyelene carbonate (EC), propylene carbonate (PC) and LiTFSI as electrolyte	• Specific capacitance of 52 mF g^{-1}. • Flammable organic electrolyte. • No tension, or bending test performed.	• Specific capacitance of 74.5 Fg^{-1}. • Aqueous electrolyte • Tension, and bending test are provided.
[18]	• Carbon nano tube, polyaniline decorated CF electrodes. • Poly ethylene glycol-solid polymer electrolyte	• Low energy density of 17.4 mWh kg^{-1}. • Flexural strength of only 21.32 MPa, no tension test	• Max energy density of 33.12 Wh kg^{-1}. • Max Flexural strength of 887.90 MPa. Tension test done
[19]	• Graphene nanoplatelets on CF as electrodes. • diglycidylether of bisphenol A epoxy with $LiClO_4$/PC as electrolyte	• Volumetric capacitance of 118.7 mF cm^{-3} • Max. Energy density of 0.2638 mWh cm^{-3}	• Max volumetric Capacitance of 14.88 F cm^{-3} • Max Energy density of 8.264 mWh cm^{-3}

[20]	• Graphene nanoplatelets and carbon aerogel modified CF • diglycidylether of bisphenol A epoxy with $LiClO_4$/PC as electrolyte	• Volumetric capacitance (C) of 79.80 mF cm^{-3} • Energy density of 0.8 Wh kg^{-1} • Flammable Organic electrolyte	• Volumetric Capacitance (C) of 14.88 F cm^{-3} • Max Energy density of 33.12 Wh kg^{-1} • Non-Flammable aqueous electrolyte
[21]	• Urea activated graphene nanoflakes grown on CF • Poly (ethylene glycol) diglycidyl ether + Ionic Liquid	• Vol. C of 82.25 mF cm^{-3} • Energy density of 0.067 mWh kg^{-1} • Use of expensive ionic liquid	• Vol. C of 14.88 F cm^{-3} • Max Energy den. Of 33.12 Wh kg^{-1} • Use of inexpensive aqueous electrolyte
[22]	• CuO nanowires on CF electrodes. • LiTf +Ionic liquid	• Grav. Cap. of 6.75 F g^{-1} • Energy density of 106.04 mWh kg^{-1} • Use of expensive ionic liquid	• Grav. Cap. of 74.5 F g^{-1} • Max Energy density of 33.12 Wh kg^{-1} • Use of inexpensive aqueous gel electrolyte
[23]	• ZnO nanotube coated CF electrodes. • LiTf+Ionic liquid	• Grav. Cap. of 10.6 F g^{-1} • Energy density of 102.69 mWh kg^{-1} • Use of expensive ionic liquid	• Grav. Cap. of 74.5 F g^{-1} • Max Energy density of 33.12 Wh kg^{-1} • Use of inexpensive aqueous gel electrolyte
[24]	• Cu-Co-Se nanowire grown on CF electrode • Polyester resin infused-LiTf-Ionic liquid	• Grav. Cap. of 28.6 F g^{-1} • Energy density of 191 mWh kg^{-1} • Use of expensive ionic liquid	• Grav. Cap. of 74.5 F g^{-1} • Max Energy density of 33.12 Wh kg^{-1} • Use of inexpensive aqueous gel electrolyte
[25]	• Lithium iron phosphate on Al foil (+ve) and CF on Cu foil (-ve) • EC and PC organic solvent with LiTf	• Energy density of 24 Wh kg^{-1} • Tensile strength of 300 MPa and no data for Bend test • Flammable organic electrolyte	• Max Energy density of 33.12 Wh kg^{-1} • Max Tensile strength of 552 MPa. Bend test data avilable • Non-flammable aqueous electrolyte.

3. References

[1] A. Riccio, C. Palumbo, V. Acanfora, A. Sellitto, A. Russo, Journal of Composites Science **2021**, 5, 310.

[2] J. Gu, P. Chen, Composite Structures **2017**, 182, 143.

[3] F. Yang, F. Yi, W. Xie, Mechanics of Materials **2021**, 160, 103928.

[4] G. Alfano, M. Crisfield, International journal for numerical methods in engineering **2001**, 50, 1701.

[5] A. Turon, P. P. Camanho, J. Costa, C. Dávila, Mechanics of materials **2006**, 38, 1072.

[6] P. P. Camanho, C. G. Dávila, **2002**.
[7] F. Chen, Y. Peng, X. Chen, K. Wang, Z. Liu, C. Chen, Polymers **2021**, 13, 604.
[8] M. L. Benzeggagh, M. Kenane, Composites science and technology **1996**, 56, 439.
[9] K. Takamoto, T. Ogasawara, H. Kodama, T. Mikami, S. Oshima, K. Aoki, R. Higuchi, T. Yokozeki, Composites Part A: Applied Science and Manufacturing **2021**, 145, 106365.
[10] E. Lindgaard, B. Bak, J. Glud, J. Sjølund, E. Christensen, Engineering Fracture Mechanics **2017**, 180, 229.
[11] C. Davila, P. Camanho, M. de Moura, "Mixed-mode decohesion elements for analyses of progressive delamination", presented at *19th AIAA applied aerodynamics conference*, **2001**.
[12] D. Pandey, K. Sambath Kumar, L. N. Henderson, G. Suarez, P. Vega, H. R. Salvador, L. Roberson, J. Thomas, Small **2022**, 2107053.
[13] R. Reece, C. Lekakou, P. A. Smith, Acs Appl Mater Inter **2020**, 12, 25683.
[14] Y. Wang, X. Qiao, C. Zhang, X. Zhou, Journal of Energy Storage **2019**, 26, 100968.
[15] Y. Xu, S. Pei, Y. Yan, L. Wang, G. Xu, S. Yarlagadda, T.-W. Chou, Acs Appl Mater Inter **2021**, 13, 11774.
[16] A. S. Westover, B. Baer, B. H. Bello, H. Sun, L. Oakes, L. M. Bellan, C. L. Pint, Journal of Materials Chemistry A **2015**, 3, 20097.
[17] N. Shirshova, H. Qian, M. S. Shaffer, J. H. Steinke, E. S. Greenhalgh, P. T. Curtis, A. Kucernak, A. Bismarck, Composites Part A: Applied Science and Manufacturing **2013**, 46, 96.
[18] N. S. Hudak, A. D. Schlichting, K. Eisenbeiser, J Electrochem Soc **2017**, 164, A691.
[19] A. Javaid, M. B. Zafrullah, F. u. H. Khan, G. M. Bhatti, Journal of Composite Materials **2019**, 53, 1401.
[20] A. Javaid, M. Irfan, Mater Res Express **2018**, 6, 016310.
[21] A. Ganguly, A. Karakassides, J. Benson, S. Hussain, P. Papakonstantinou, Acs Appl Energ Mater **2020**, 3, 4245.
[22] B. K. Deka, A. Hazarika, J. Kim, Y.-B. Park, H. W. Park, Composites Part A: Applied Science and Manufacturing **2016**, 87, 256.
[23] B. K. Deka, A. Hazarika, O. Kwon, D. Kim, Y.-B. Park, H. W. Park, Chem Eng J **2017**, 325, 672.
[24] B. K. Deka, A. Hazarika, J. Kim, N. Kim, H. E. Jeong, Y.-B. Park, H. W. Park, Chem Eng J **2019**, 355, 551.
[25] L. E. Asp, K. Bouton, D. Carlstedt, S. Duan, R. Harnden, W. Johannisson, M. Johansen, M. K. Johansson, G. Lindbergh, F. Liu, Advanced Energy and Sustainability Research **2021**, 2, 2000093.